Morphogenetic processes as data: Quantitative structure in the *Drosophila* eye imaginal disc

Bradly Alicea[1,2], Thomas E. Portegys[2], Diana Gordon[3], Richard Gordon[4,5]

Keywords: Quantitative Methods, Drosophila, Imaginal Disc, Developmental Biology

Abstract

We can improve our understanding of biological processes through the use of computational and mathematical modeling. One such morphogenetic process (ommatidia formation in the *Drosophila* eye imaginal disc) provides us with an opportunity to demonstrate the power of this approach. We use a high-resolution image that catches the spatially- and temporally-dependent process of ommatidia formation in the act. This image is converted to quantitative measures and models that provide us with new information about the dynamics and geometry of this process. We approach this by addressing three computational hypotheses, and provide a publicly-available repository containing data and images for further analysis. Potential spatial patterns in the morphogenetic furrow and ommatidia are summarized, while the ommatidia cells are projected to a spherical map in order to identify higher-level spatiotemporal features. In the conclusion, we discuss the implications of our approach and findings for developmental complexity and biological theory.

Introduction

To advance the development and use of computational representations and models in developmental neuroscience, we require a well-characterized biological system that yields fairly unambiguous information regarding the differentiation process. We propose that the eye imaginal disc of the fruit fly (*Drosophila melanogaster*) is such a candidate system. In the *Drosophila* eye imaginal disc, ommatidia differentiation proceeds anteriorly from left (posterior) to right (anterior), and commences at the beginning of the third instar. It is an autoregulatory process that relies upon a complex network of molecular signals (Roignant and Treisman, 2009) triggered by a traveling induction wave (morphogenetic furrow), which has previously been classified as a Type 2 differentiation wave with an alternating pattern of differentiation (Gordon and Gordon, 2016) controlling both the timing and positions of differentiated cells.

In the eye imaginal disc, we seek to understand the differentiation process relative to the morphogenetic furrow. The morphogenetic furrow is a structure that is defined by apical constriction and apical-basal contraction (Gordon and Gordon, 2016; Lee and Treisman, 2002; Schlichting and Dahmann, 2008). This furrow produces 800 ommatidia structures present in the adult compound eye by inducing proneural states during its movement through undifferentiated cells (Chanut and Heberlein, 1995). The cells in this epithelium commit to a neuronal fate as they receive signals triggered by the passing of the morphogenetic furrow and its proximity to/recruitment by an ommatidia founder (R8) cell (Brennan and Moses, 2000; Dokucu et al., 1996). Yet not all cells in this sheet commit to a neuronal fate (Wolff and Ready, 1991), and we

1 Orthogonal Research and Education Laboratory, Champaign IL USA (bradly.alicea@outlook.com)
2 OpenWorm Foundation, Boston, MA USA
3 Healdsburg CA 95448-4864 USA
4 Gulf Specimen Marine Laboratory & Aquarium, Panacea, FL USA
5 C.S. Mott Center for Human Growth & Development, Department of Obstetrics & Gynecology, Wayne State University, Detroit MI USA

characterize these as background cells. While quite regular, this process also reveals a degree of intrinsic variation (Swain et al., 2002) between eye imaginal discs. Various molecular pathways interact with progression of the furrow during differentiation of various cells in a single ommatidium (Davis and Rebay, 2018; Greenwood and Struhl, 1999). These differentiations may be due to we have called single-cell differentiation waves (Gordon and Gordon, 2016; Gordon, 1999).

Our data consists of a single, high-resolution camera obscura drawing of a *Drosophila melanogaster* eye imaginal disc observed during the third instar of development (Wolff, 1993). These data are unique in that the imaginal disc has been caught in the act of differentiating with every cell recorded (Figure 1). A morphogenetic furrow marks the boundary between a population of isotropic and undifferentiated cells to a structured population of ommatidia cells and background cells. Here we use both mathematical and computational techniques to uncover the patterns, features, and geometric relationships previously not characterized in the literature. This type of systems morphometrics has the potential to inform molecular investigations, as well as computer simulations of the developing *Drosophila* eye.

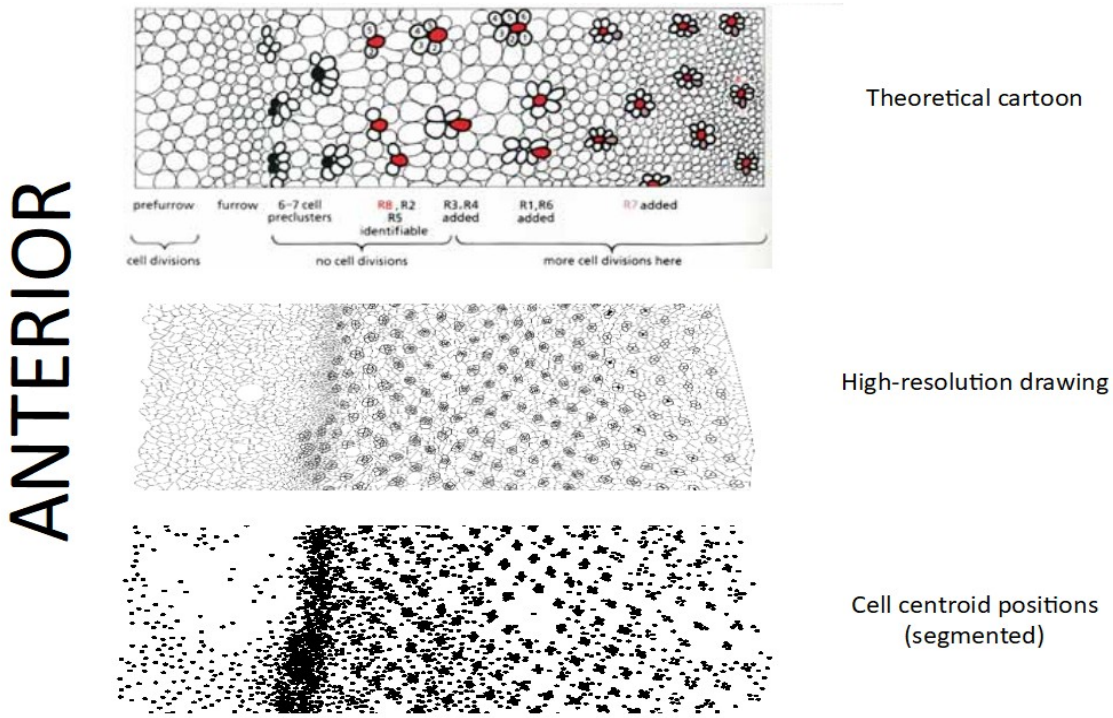

Figure 1. Diagram showing movement of furrow towards anterior end of eye imaginal disc. **Top:** labeled diagram of the whole process with key cell types labeled. **Middle:** a strip from our corrected high-resolution drawing. **Bottom:** a strip from a segmented set of cells, with centroids marked by black dots.

In addition to applying a series of quantitative techniques, we also wish to establish an open dataset as well as to extract information about a single developmental process. A previous analysis of these data only estimated one visually invisible, global pattern, an alternation of 2 large/2 small cells along the bottom of the furrow, using a variogram method (Gordon, 1999). Our approach here is much more comprehensive, and applies image processing techniques, feature selection methods, and geometrical transformations to the same source material. This

paper presents an exploratory analysis of the data along with four computational hypotheses, the latter of which may ultimately lead to both local and global statistical invariants.

Computational Hypotheses

We propose four computational hypotheses that can be realized through analysis and transformation of the quantitative data. We will address these hypotheses using a variety of methods. These can be stated as follows:

H1: the size distributions of cells representing three components of the eye imaginal disc (furrow, differentiated background, and ommatidia) will yield differences.

H2: characterizing ommatidia complexity (size and position) can be informative for understanding the tempo of differentiation in both space and time.

H3: projecting ommatidia to a spherical map can provide a uniform representation on which to model the process of differentiation.

H4: animations of the spherical map as a series of time slices will reveal a process analogous to anatomical differentiation.

Methods

The poster accompanying Wolff (1993) was digitized and the loops, representing cell boundaries, were closed digitally by hand, where needed, as shown in Figure 2. The retouched and digitized image is shown in Supplemental File 1. By comparing our digitized image showing about 150 pixels between ommatidia with Figure 11 in Wolff and Ready (1993), with an average distance between adjacent ommatidia of 7.2 µm, we estimate the width of our pixels at 0.05 µm. The image was then inverted and segmented using the ImageJ (NIH; Bethesda, MD USA) particle analysis function. This resulted in discrete cells (n=9733) each with a defined area and 2-D centroid position. Inspection of the inverted image suggested that all cells were segmented from one another. The segmented image was further transformed using two types of transformation: spherical projection and realignment. Realignment was achieved by using a linear regression function to align the image about the central region of the morphogenetic furrow identified by cell density and the ends of ommatidia rows defined through a ridge estimation. The retouched image was also decomposed manually into layers containing 1) cells associated with the ommatidia, 2) cells serving as the background to the ommatidia and anterior to the furrow, and 3) cells associated with the furrow. Layers were defined by transitions in pattern, cell size and line thickness.

Open Data and Analysis

We have provided extensive documentation of our data and analysis in a collaborative online repository. Anyone can become a collaborator and contribute to the analysis set. All code, analyses, and associated images are publicly available on Github: https://github.com/devoworm/Drosophila-imaginal-disc-segmentation.

Binary Maps

Binary maps were created and are in the publicly-available repository. All images were reduced to a 1-bit binary images and decomposed into a numeric matrix, with pixels labeled “1” being cells of interest and pixels labeled “0” being background cells. Ommatidia and background layers were decomposed into binary maps and reconstructed using SciLab 6.0 (Paris, France) and

the IPCV 1.2 toolbox (http://scila.pcv.tritytech.com). Binary maps were used to verify segmented images and their relationship in the ommatidia.

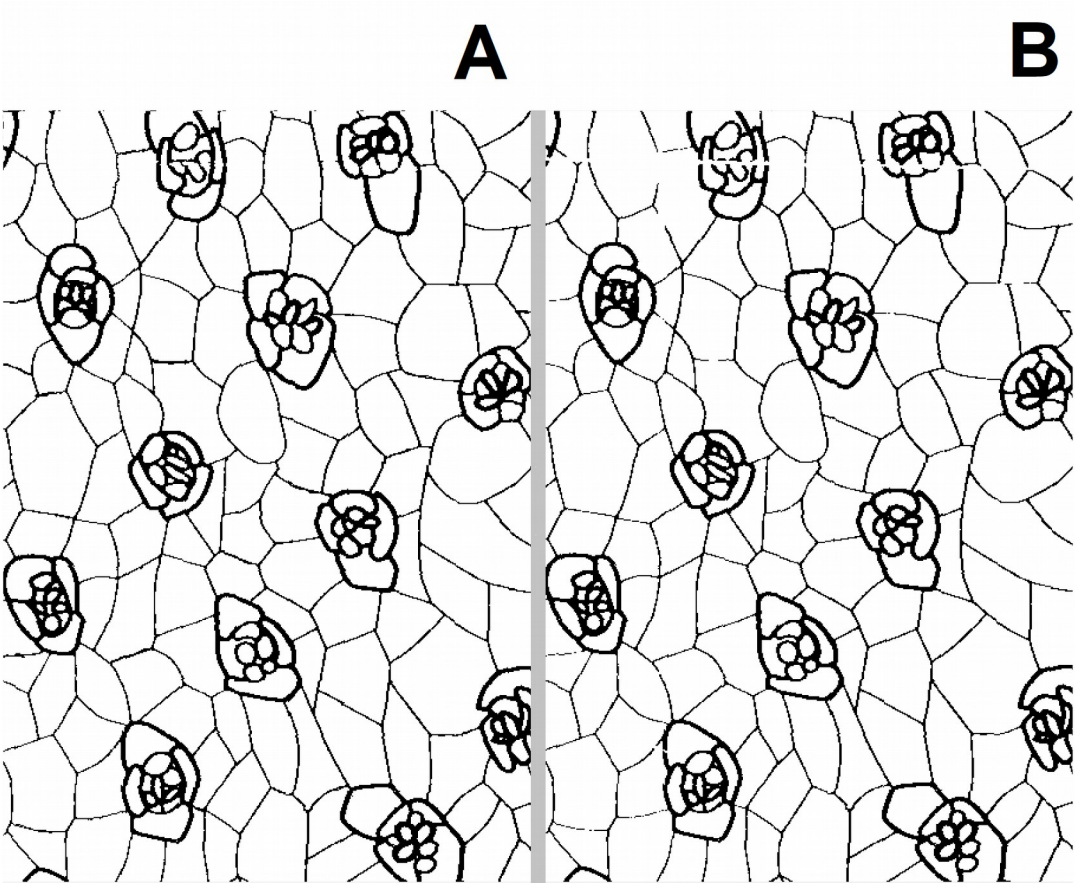

Figure 2. Closeup of the camera obscura sketch of all cells in a *Drosophila* imaginal disc (Wolff, 1993). **A:** before correction. **B:** after closing by hand all cell-cell boundaries that had gaps. For the full, corrected sketch see the Supplement File 1. Note that the original sketch had thick lines designating ommatidial cells.

All binary maps are presented in the Github repository. Binary maps for "BG-left" and "ommatidia" were created from the "background" and "ommatidia" masks as described in the Methods section. Each mask was reduced to a 1-bit image in ImageJ, then converted into a binary matrix using SciLab 6.0. Binary images describe every pixel that belong to a cell, and were coded with a value of "1". This binary matrix can be reduced to a set of x,y coordinates for which the color value equals "1" using the SciLab code in files "code-for-binary-images.md" and "ht-make-xy-points-from-binary-matrix.md".

Discrete Feature Spaces

To identify specific features in the segmented data, we created several layers which were then used to segment and label specific types of features. These layers included the furrow layer (n=1433), the background layer (n=3966), and the ommatidia layer (n=3811). The remaining 523 cells are prefurrow cells (Figure 1). The ommatidia layer was later limited to all cells larger than 100 pixels (n=3249). The most informative of these is the ommatidia layer, which features only cells associated with ommatidia and form multiple rows across the differentiated surface of the imaginal disc. A labeled dataset was created from the ommatidia layer and included all

segmented cells over 100 pixels in size. Each cell was assigned to a cluster, which was labeled by row and order from anterior to posterior.

Furrow Alignment

A linear regression function was used to align and rotate the segmented imaginal disc about the furrow to represent the furrow as a straight vertical line. Using 18 candidate points estimated from center of the furrow layer, a linear regression equation was calculated. The a and b parameters were then optimized until a straight line was obtained. The optimal function is: $y = 11.57 + 9722.8x$. All x and y coordinates were then transformed to x' and y' using the following equations

$$x' = 11.57x - 9722.8 \quad [1]$$

$$y' = \frac{9722.8 + x}{11.57} \quad [2]$$

We have also developed software to straighten the furrow using a different methodology. While this alternate method straightens the eye imaginal disc furrow in the raw (unsegmented image), it also introduces waviness in the cell bodies. This program is located in the public Github repository.

Ridge Estimation

To determine which cell clusters constituted rows of ommatidia, ridges were estimated from a scatterplot of all cells anterior to the morphogenetic furrow. A ridge can be defined as an n^{th} order polynomial function that passes through an aligned series of cell clusters. Clusters are defined as regions of high density in the scatterplot, or regions where more than 10 centroids are fused together in the image.

Spherical Map

The realigned ommatidia were mapped to a spherical representation, which provides a space within which to explore the data:

$$v_x = \cos(x) * \cos(y) \quad [3]$$

$$v_y = \cos(x) * \sin(y) \quad [4]$$

$$v_z = \sin(x) \quad [5]$$

Spherical Map Spatial Animations

To understand potential patterns in the spatial process, ommatidia cells were stratified into nine (9) spatial regions of uniform size (based on the range of x-axis positions in the data), which also represent discrete periods of time since differentiation. Generally, the farther the cells are to the anterior, the older they are. Spatial positions were taken from aligned x,y coordinates and then projected to the spherical map with cell size information added. A series of nine graphs with cells from their corresponding spatial division were plotted in SciLab 6.0 (Paris, France) and used to build two animations. A slow animation (350 ms latency between the individual plots) is contrasted with a fast animation (50 ms latency between the individual plots).

Analysis

Cell Size Distributions

To get a feel for the segmented data, we constructed a rank-order frequency plot that shows a relationship many small cells and relatively fewer large cells. Figure 3 shows the data for all segmented cells in the eye imaginal disc. The graph shows not only the expected preponderance of smaller cells, but also the range of variation at smaller sizes (Figure 3 inset). One notable feature of this distribution is a diversity of sizes that is consistent both among smaller and larger cells. This may be related to the independence of differentiation waves from cell size, as is apparent in polyploid axolotls (Gordon and Gordon, 2016). The cause of the wide range of cell sizes in the *Drosophila* eye imaginal disc is not known.

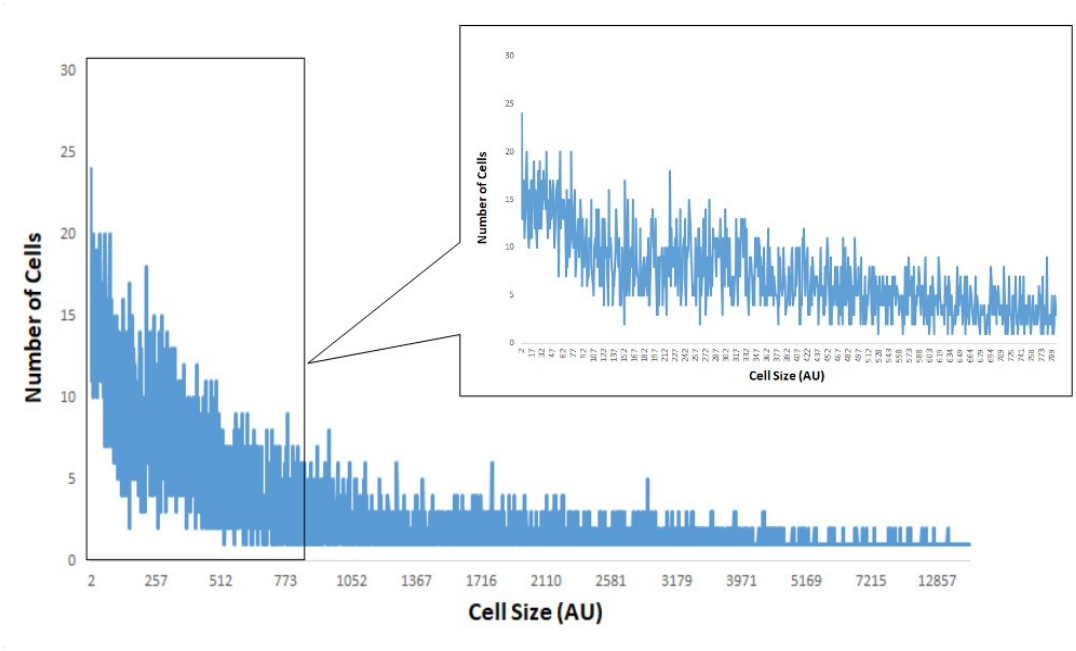

Figure 3. MAIN: Rank order frequency plot (exponential distribution) for all cells in the non-normalized eye imaginal disc segmentation. **INSET:** A subset of cells (ranging from size 2 to 800 pixels) that serves as a close-up of the support for this distribution. In the main plot, all cells of size 1 and greater than size 40000 were eliminated to minimize statistical artifact. The small "cells" may be noise artifacts of the segmentation algorithm.

To follow up on the diversity signatures, we also looked at a more restricted set of regions within the eye imaginal disc. The cell size distribution of the isolated furrow, isolated background, and isolated ommatidia were calculated and compared. This was done using three histograms, and the analysis shows differences in cell size between each region in shown in Figure 4.

A comparison between the histograms does reveal a few trends worth noting. Cells labeled as "background" tend to have many very small constituents, while those labeled "furrow" and "ommatidia" have a bit more size diversity. Notably, the furrow has a bit more diversity at larger size scales, but in a different way than the bulk size distribution. These size distributions challenge the view of the eye imaginal disc as a "crystalline" array (Ready et al., 1976).

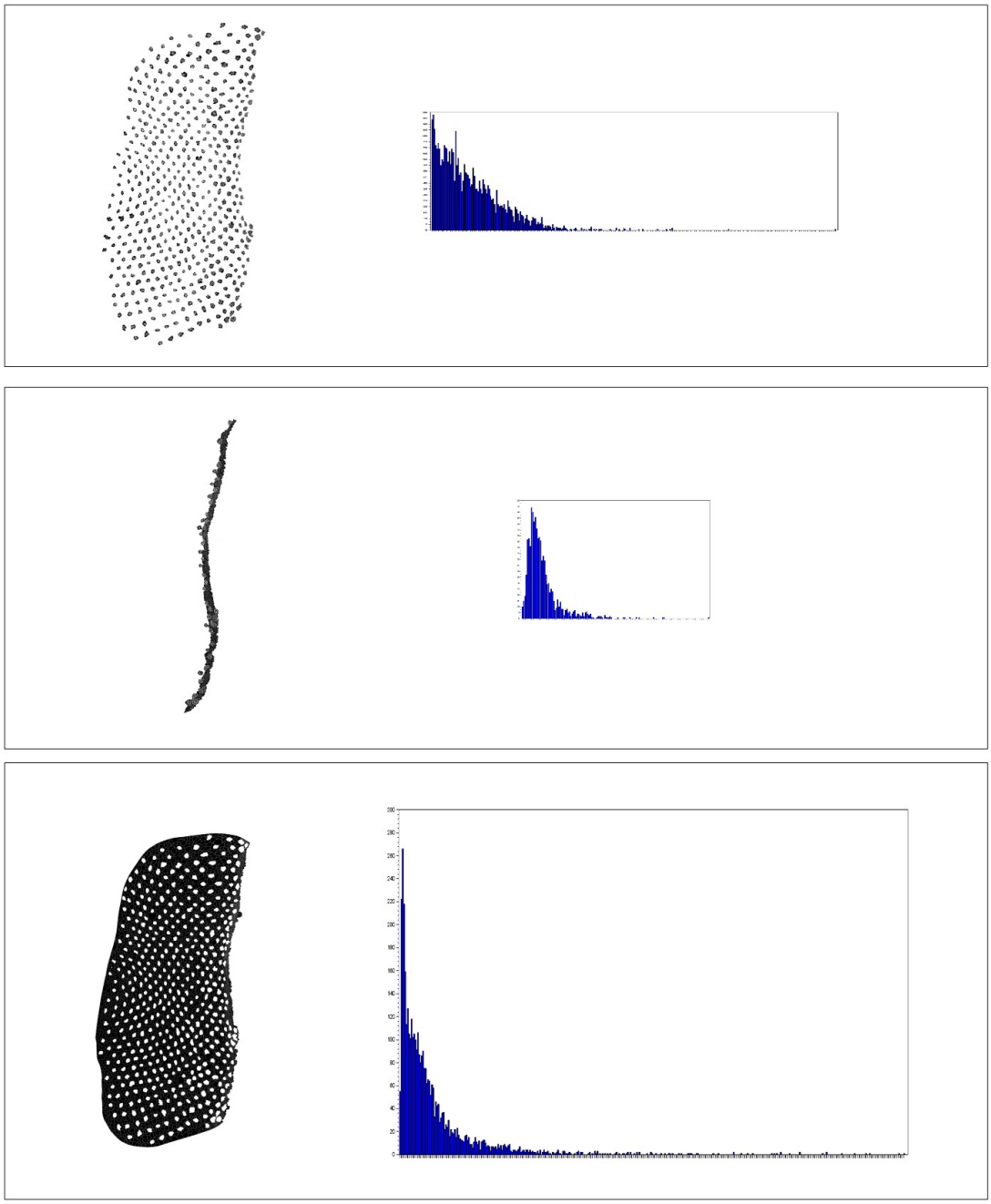

Figure 4. A: isolated ommatidia, **B:** isolated furrow, **C:** isolated background cells. Histograms containing ***D*:** isolated ommatidia (n=3249, 325 bins), ***E*:** isolated furrow (n=1433, 143 bins), ***F*:** isolated background (n=3966, 397 bins). Bin sizes were chosen to have approximately the same number of cells in each bin across all cell types. Histograms have been scaled the same way for comparison.

Furrow Straightening

One strategy used to correct for curvature of the furrow in the original specimen is to find a canonical furrow and align all cells to the linear function. This is done using a linear regression function to realign the cells. A plot of the non-layered realigned eye imaginal disc and alignment function are shown in Figure 5.

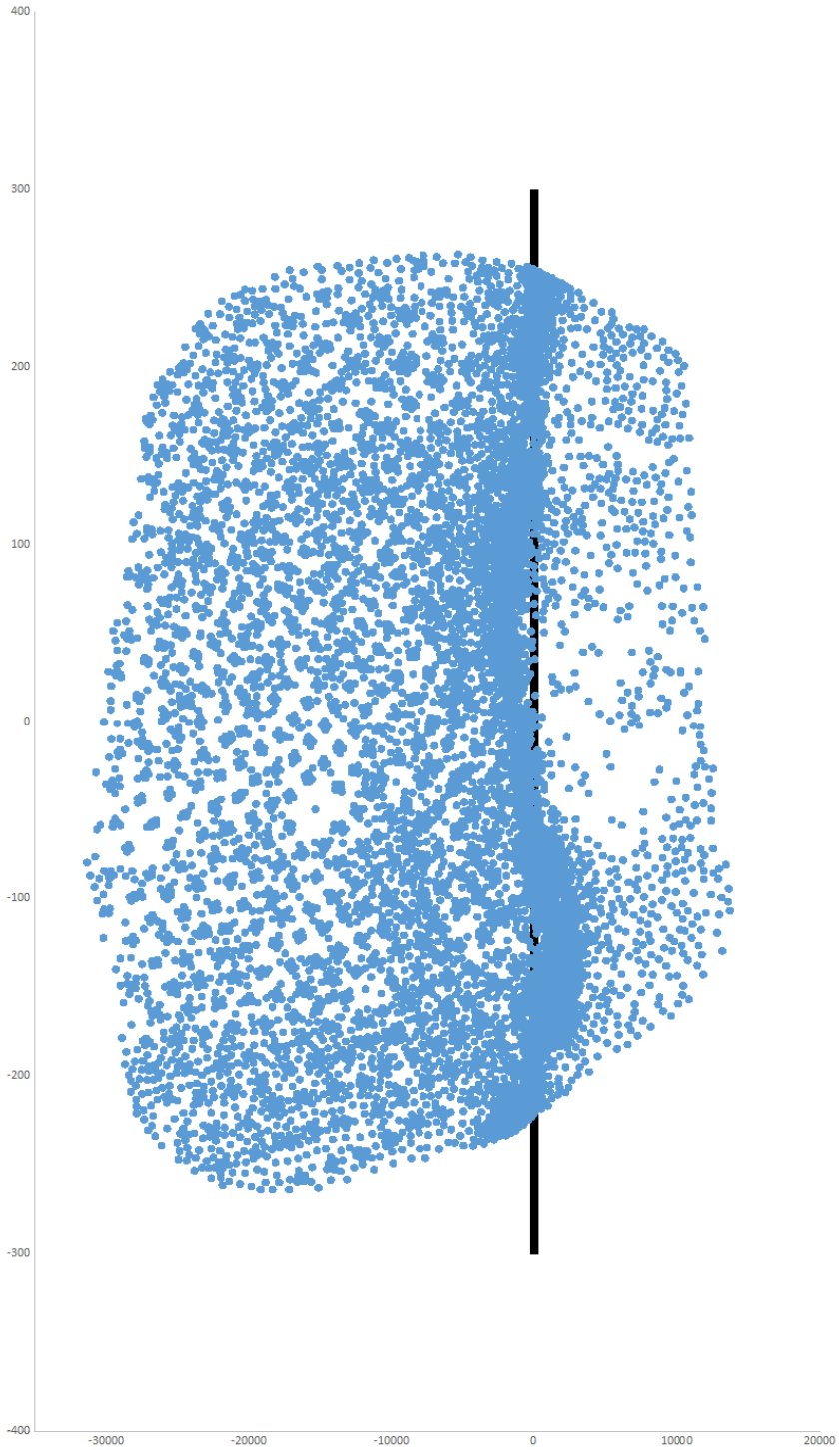

Figure 5. Image of the segmented eye imaginal disc centered upon an vertical line that runs through the mean of the furrow region. **Blue dots:** cell centroids, **Black line:** central axis of furrow.

In Figure 5, we can clearly identify centroids marking individual ommatidia. These centroids (representing cells of different sizes) appear as clusters against a background of

individual centroids or smaller clusters. The relatively large size and alignment of these ommatidia-related clusters allows us to apply an estimation procedure to identify larger-scale features such as sequential rows of ommatidia. We use an approach called ridge estimation to make these identifications.

Ridge Estimation in the Differentiated Region

Using all segmented cells (centroids) to the anterior (differentiated region) of the furrow region, ridges were estimated for all centroid clusters in the image (Figure 6). These centroid clusters were used to determine the positions of individual ommatidia (see Methods).

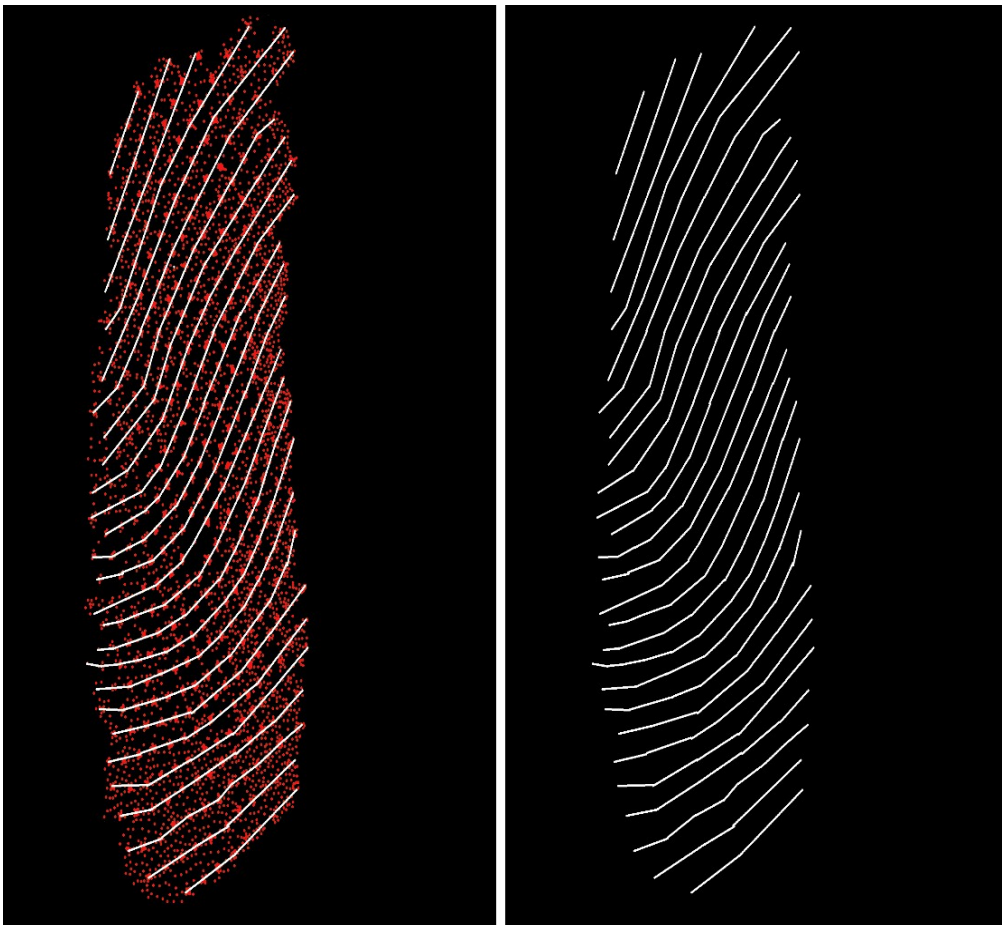

Figure 6. Ridge estimates that reveal 26 distinct rows of ommatidia across the differentiated section of the eye imaginal disc. **LEFT:** ridge estimation from segmented centroids. **RIGHT:** ridges in isolation demonstrating the estimated contours of each row.

Characterizing Ommatidia Complexity

To understand the labeled ommatidia cells in more detail, we quantified individual ommatidium and compared them across individual rows and columns. A statistical summary of each ommatidium is presented in Supplemental File 2.

Projections to Spherical Map

To understand patterns in the ommatidia feature space and to reduce the multidimensional effects of ommatidia ridge curvature, the data were projected to a spherical coordinate system. These data were then plotted and shown in Figure 7.

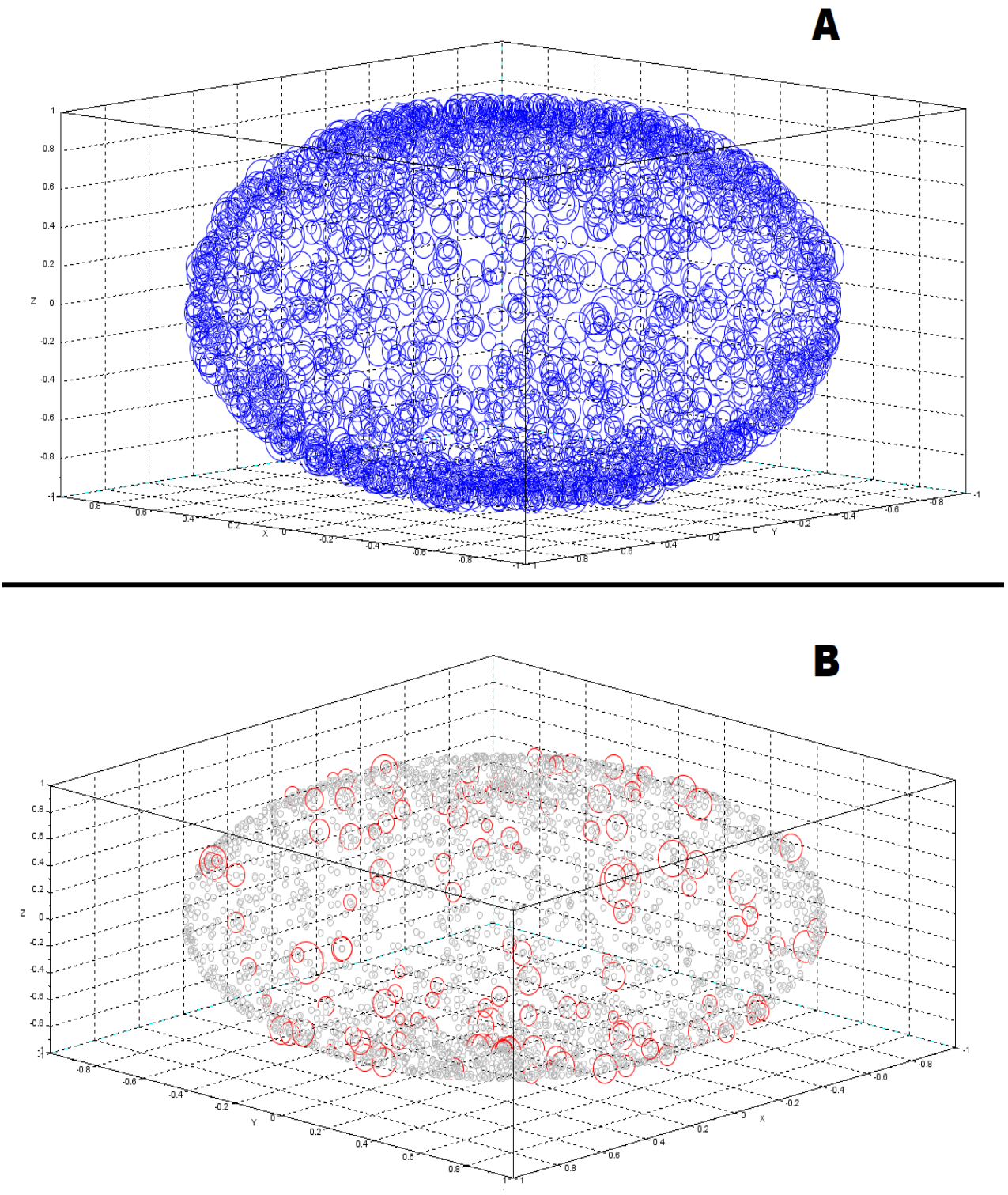

Figure 7. Ommatidia feature space projected to a spherical transformation. **A:** ommatidia cells transformed to a spherical map and plotted by shape. **B:** cells for all row 8 ommatidia as identified in Appendix A plotted on spherical map relative to their size (red circles). Note that this display software squishes the sphere.

These data can also be stratified to show patterns and relationships between different classes of cells. Supplemental Files 3 and 4 demonstrate how differentiation over time can be represented in both slow (SF3) and fast (SF4) animations. Supplemental File 3 and Supplemental File 4 are projected at 350 ms latency and 50 ms latency, respectively (see Methods). In the fast animation, it appears that a dipole pattern emerges on the sphere from the first stage to the last stage which is reinforced upon looping. This may have relevance to the spatial unfolding of differentiation, and how the ommatidia in the non-projected layer (real space) seem to curve upward in areas adjacent to the morphogenetic furrow.

Discussion

The developmental process results in a number of spatial patterns. Some of these patterns describe differentiation as it unfolds. Other patterns reflect meta-features of the embryo at multiple spatial scales that might be biologically informative. One of our primary motivations comes from Proposition 250 as introduced in Gordon (1999). Proposition 250 states that the spacing patterns of cells (relative size and position) are indicative of contraction and expansion waves that occur during development. While more work needs to be done to make definitive statements about this proposition with respect to *Drosophila* eye imaginal disc, we suspect that the there is an interaction between the morphogenetic furrow and the relative location of differentiated cells (Courcoubetis et al., 2018).

We have proposed a series of quantitative approaches for understanding the interesting developmental properties of the *Drosophila* eye imaginal disc. We have also addressed our four computational hypotheses. The spherical map provides a uniform space where spatial variation due to artificial sources of curvature are removed. Further analysis of the data embedded in this structure is necessary to make more comprehensive statements about relationships between different regions of the ommatidia array.

While the ridge estimation procedure was used to yield labeled series for ommatidia rows, the analysis of the resulting graph might be the object of future work. As these ridge maps resemble fingerprint patterns, mathematical techniques for their analysis with broad application might be possible. Such an analysis also reveals new statistical features as well as local patterns in information content relevant to fluctuations in the developmental process. The independence of the ommatidia pattern from the wide range of cell sizes is particularly noteworthy.

There are a number of additional approaches that might be used in the future to uncover further developmental complexity. Our measurement of labeled ommatidia cell size resembles the ensemble averages of Torquato and Stillinger (2003) in their method to detect hyperuniformity of features in a spatial array. While we did not look for hyperuniformity amongst ommatidia structures, models of hyperuniformity and neural selection (Frankfort and Mardon, 2002) might be used to find additional patterns in these data. We can also look at other developmental systems (such as the development of horns in insects) for principles of developmental morphogenesis (Matsuda et al., 2017).

The Drosophila eye imaginal disc deserves further time lapse analysis, well beyond what we could do here with a single camera lucida drawing. For instance, the shibire mutant results in broad lines of no ommatidial formation when the temperature is raised, but ommatidia continue to form when it is lowered. If the temperature is raised, lowered, then raised and lowered again, two smooth broad lines are formed (Suzuki, 1974) (Figure 8). This suggests that the morphogenetic furrow, and perhaps differentiation waves in general, can be uncoupled from differentiation itself,

and offers a powerful tool for investigating whether or not differentiation waves are actually causal of cell differentiation, as we have proposed (Gordon and Gordon, 2016; Gordon, 1999)

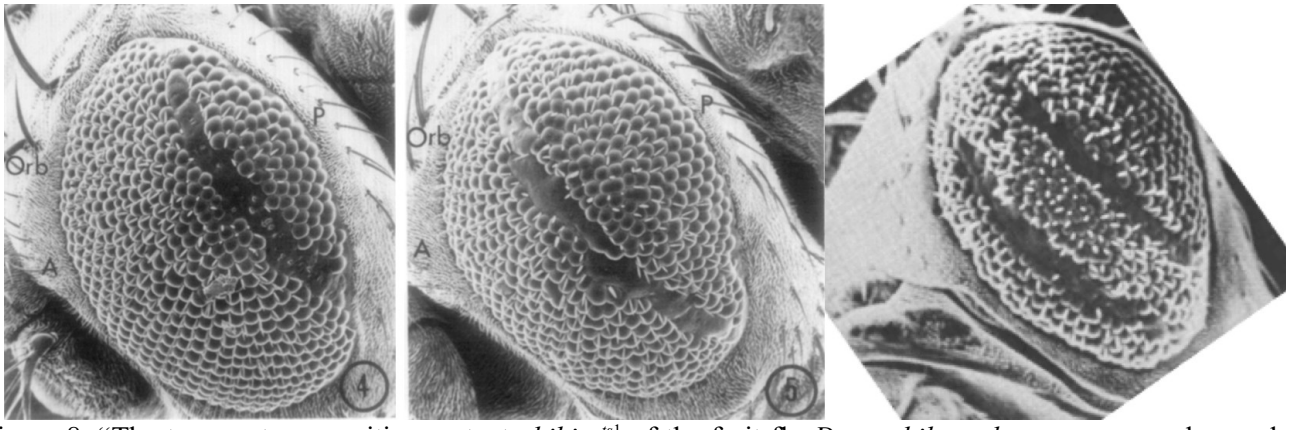

Figure 8. "The temperature sensitive mutant *shibire*^{ts1} of the fruit fly *Drosophila melanogaster* may be used to record the motion of the differentiation wave called the 'morphogenetic furrow' across the eye imaginal disc. **Left**: When the temperature is raised briefly from 22 to 29°C the wave keeps propagating, but the subsequent steps of differentiation of the cells into ommatidia fail. **Middle**: Here the temperature was raised briefly at a later time. The first two SEMs are from Poodry et al. (1973) with permission of Elsevier. **Right**: When the temperature is raised briefly twice, two lines of ommatidia are missing. The third SEM is rotated to the same orientation of the first two and is from Suzuki (1974) with permission of NRC Research Press" (Gordon and Gordon, 2016). Anterior is to the upper right.

Supplemental Material

Supplemental File 1. Retouched and digitized drawing of the eye imaginal disc. Original drawing made by Dr. Tanya Wolff (Wolff, 1993), image retouching done by Diana Gordon.

Supplemental File 2. Summary statistics (Counts, mean size, and mean position for all ommatidia labeled by their row and order from the posterior to the anterior side of the imaginal disc.

Supplemental File 3. Slow animation (350 ms latency) of ommatidia formation on the spherical map.

Supplemental File 4. Fast animation (50 ms latency) of ommatidia formation on the spherical map.

References

Brennan, C.A., Moses, K., 2000. Determination of *Drosophila* photoreceptors: Timing is everything. Cell Mol Life Sci 57(2), 195-214.

Chanut, F., Heberlein, U., 1995. Role of the morphogenetic furrow in establishing polarity in the *Drosophila* eye. Development 121(12), 4085-4094.

Courcoubetis, G., Ali, S., Nuzhdin, S.V., Marjoram, P., Haas, S., 2018. Threshold Response to Stochasticity in Morphogenesis. http://adsabs.harvard.edu/abs/2018arXiv180401696C

Davis, T.L., Rebay, I., 2018. Pleiotropy in *Drosophila* organogenesis: Mechanistic insights from Combgap and the retinal determination gene network. Fly 12(1), 62-70.

Dokucu, M.E., Zipursky, S.L., Cagan, R.L., 1996. Atonal, Rough and the resolution of proneural clusters in the developing *Drosophila* retina. Development 122(12), 4139-4147.

Frankfort, B.J., Mardon, G., 2002. R8 development in the *Drosophila* eye: A paradigm for neural selection and differentiation. Development 129(6), 1295-1306.

Gordon, N.K., Gordon, R., 2016. Embryogenesis Explained. World Scientific Publishing, Singapore.

Gordon, R., 1999. The Hierarchical Genome and Differentiation Waves: Novel Unification of Development, Genetics and Evolution. World Scientific & Imperial College Press, Singapore & London.

Greenwood, S., Struhl, G., 1999. Progression of the morphogenetic furrow in the *Drosophila* eye: the roles of Hedgehog, Decapentaplegic and the Raf pathway. Development 126(24), 5795-5808.

Lee, J.D., Treisman, J.E., 2002. Regulators of the morphogenetic furrow, *Drosophila* Eye Development. Springer, pp. 21-33.

Matsuda, K., Gotoh, H., Tajika, Y., Sushida, T., Aonuma, H., Niimi, T., Akiyama, M., Inoue, Y., Kondo, S., 2017. Complex furrows in a 2D epithelial sheet code the 3D structure of a beetle horn. Sci Rep 7, #13939.

Poodry, C.A., Hall, L., Suzuki, D.T., 1973. Temperature-sensitive mutations in *Drosophila melanogaster*. Part XV. Developmental properties of *shibire*^{ts1}: a pleiotropic mutation affecting larval and adult locomotion and development. Dev. Biol. 32(2), 373-386.

Ready, D.F., Hanson, T.E., Benzer, S., 1976. Development of the *Drosophila* retina, a neurocrystalline lattice. Dev. Biol. 53, 217-240.

Roignant, J.-Y., Treisman, J.E., 2009. Pattern formation in the *Drosophila* eye disc. Int. J. Dev. Biol. 53(5-6), 795-804.

Schlichting, K., Dahmann, C., 2008. Hedgehog and Dpp signaling induce cadherin Cad86C expression in the morphogenetic furrow during *Drosophila* eye development. Mech. Dev. 125(8), 712-728.

Suzuki, D.T., 1974. Behavior in *Drosophila melanogaster*: a geneticist's view. Canadian Journal of Genetics and Cytology 16(4), 713-735.

Swain, P.S., Elowitz, M.B., Siggia, E.D., 2002. Intrinsic and extrinsic contributions to stochasticity in gene expression. Proc. Natl. Acad. Sci. U. S. A. 99(20), 12795-12800.

Torquato, S., Stillinger, F.H., 2003. Local density fluctuations, hyperuniformity, and order metrics [+ correction **68**(6), #069901]. Physical Review E 68(4), #041113.

Wolff, T., 1993. *Drosophila* third instar eye disc, In: Bate, M., Martinez Arias, A. (Eds.), The Development of *Drosophila melanogaster*. Cold Spring Harbor Laboratory Press, Plainview, New York, p. poster in pocket.

Wolff, T., Ready, D.F., 1991. The beginning of pattern formation in the *Drosophila* compound eye: the morphogenetic furrow and the second mitotic wave. Development 113(3), 841-850.

Wolff, T., Ready, D.F., 1993. Pattern formation in the *Drosophila* retina, In: Bate, M., Martinez Arias, A. (Eds.), The Development of *Drosophila melanogaster*, Vols. 1 and 2. Cold Spring Harbor Laboratory Press, Plainview, New York, USA, pp. 1277-1325.